

Liquid crystal Pancharatnam-Berry phase lens with spatially separated focuses

Yaqin Zhou, Yue Yin, Yide Yuan, Tiegang Lin, Huihui Huang, Lishuang Yao, Xiaoqian Wang, Alwin M. W. Tam, Fan Fan & Shuangchun Wen


To cite this article: Yaqin Zhou, Yue Yin, Yide Yuan, Tiegang Lin, Huihui Huang, Lishuang Yao, Xiaoqian Wang, Alwin M. W. Tam, Fan Fan & Shuangchun Wen (2018): Liquid crystal Pancharatnam-Berry phase lens with spatially separated focuses, Liquid Crystals, DOI: 10.1080/02678292.2018.1550820

To link to this article: <https://doi.org/10.1080/02678292.2018.1550820>



Published online: 02 Dec 2018.



Submit your article to this journal 



Article views: 22



View Crossmark data 



Liquid crystal Pancharatnam-Berry phase lens with spatially separated focuses

Yaqin Zhou^a, Yue Yin^a, Yide Yuan^a, Tiegang Lin^a, Huihui Huang^a, Lishuang Yao^b, Xiaoqian Wang^c, Alwin M. W. Tam^d, Fan Fan^a and Shuangchun Wen^a

^aKey Laboratory for Micro-/Nano-Optoelectronic Devices of Ministry of Education, School of Physics and Electronics, Hunan University, Changsha, China; ^bState Key Laboratory of Applied Optics, Changchun Institute of Optics, Fine Mechanics and Physics, Chinese Academy of Sciences, Changchun, China; ^cPhysics Department, East China University of Science and Technology, Shanghai, China; ^dPartner State Key Laboratory on Advanced Displays and Optoelectronics Technologies, Department of Electronic and Computer Engineering, Hong Kong University of Science and Technology, Hong Kong, China

ABSTRACT

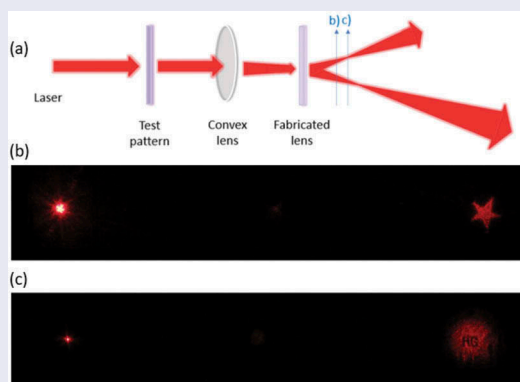
In this paper, we proposed and fabricated a liquid crystal (LC) lens with spatially separated focuses via liquid crystal photoalignment technology. The novel lens is an integration of the polarisation grating and conventional LC lens. The two focuses of that new lens, one of which is real while the other is virtual, can be spatially separated. When combined with normal convex lens and illuminated by a linearly polarised beam, the two emergent light beams become all convergent and the two focuses are separated in three-dimension space. Moreover, the focal lengths of the lens system can be artificially controlled by adjusting the distance between our new lens and the conventional lens. Our results achieve the potential of LC lens' application in imaging devices such as multifocal cameras, bifocal eyeglasses and so on.

ARTICLE HISTORY

Received 24 October 2018
Accepted 18 November 2018

KEYWORDS

Liquid crystal;
Pancharatnam-Berry phase;
lens



Lens, as one of the most important and widely used optical elements, is playing an irreplaceable role in our daily life, such as the eyeglass for correcting myopia and hyperopia, camera lens for photographing, and the microscope and telescope for observing the tiniest small and furthest distance materials and structures. Comparing with the fast-developing electronics area [1], the development of optics area is rather slow. We are still using almost the same lenses comparing with those used in Newton's time. The commonly used lenses for cameras, eyeglasses and other applications are formed by glass or plastic with curved surfaces [2,3]. With the spatial variation of thickness, the optical path difference is generated for modulating the optical-phase profile [4,5]. Due to the relatively large thickness

for the lenses, the formed optical systems are normally bulky and heavy [6], which are not well suitable for the increasing demanding for the integration and miniaturisation of modern optical systems [7].

With the development of micro/nano-fabrication technologies and new materials, new ultra-thin flat lenses are emerging, which are normally formed by micro/nano-structures, with thickness in the level nanometres or micrometres [8,9]. Compared with conventional refractive lenses, the new ultra-thin lenses show good potential to form highly integrated and compact size optical systems. There are several kinds of ultra-thin flat lenses, including the metalenses which are composed of periodic subwavelength dielectric or metal structures [10,11], and the liquid crystal (LC)

lens based on Pancharatnam-Berry (PB) phase modulation [12–14]. The metalenses are normally fabricated by techniques including electro-beam lithography and photolithography technologies [15,16], most of which are too complex, time-consuming and equipment-required, leading the metalens size limited to submillimetre size. Different from metalenses, the fabrication of LC ultra-thin lenses is based on the LC photoalignment technology [17], providing us an easier, cheaper and more convenient way to fabricate an ultra-thin lens via manipulating the optical axis orientation of the LC molecules [18,19].

For the general LC PB lens, opposite phase profile is generated according to the different handedness of the incident circularly polarised light (CPL), leading the lens to have bifocal property. The two focuses of the LC lens are on the same light path, which will result the overlapping of the two emergent light beams [20]. In this paper, we proposed and fabricated a new LC PB phase lens. Different from the conventional LC PB lens, the proposed lens can generate two spatially separated focuses with both focuses shifting out of the central axis, which can avoid the overlap of beams happened in conventional LC PB lens. With this special optical property, the lens shows good potential to be used in many applications such as polarising imaging [21,22], multifocal cameras and some other multi-channel optical systems in need of controlling the size of the generated beams or the length of the generated focused light paths at certain spatial points of interest [23,24].

The LC PB phase lenses manipulate light by the generation and modulation of the PB phase [25,26], which is in no relationship with the optical path difference but derives from the generation and manipulation of the space-variant polarisation. Those devices whose optical properties stem from the PB phase are called PB phase optical elements [27,28]. They were widely used for the shaping of various wavefronts such as helical wavefront for vortex beam [12], pyramidal-shaped wavefront for focusing or diverging beam [29], as well as for the space-variant polarisation generation and manipulation of vector beams [30,31]. When a waveplate with local direction of optical axis θ and phase retardation δ is illuminated by a CPL $E_{in} = [1 \ \sigma j]^T$, in which $\sigma = \pm 1$ represents right- and left-handedness of circular polarisation, the Jones vector of the output beam can be written as:

$$E_{out} = \cos \frac{\delta}{2} \begin{bmatrix} 1 \\ \sigma j \end{bmatrix} - j \sin \frac{\delta}{2} \exp(2\sigma\theta j) \begin{bmatrix} 1 \\ -\sigma j \end{bmatrix}. \quad (1)$$

When the waveplate is a half waveplate with $\delta = \pi$, the output beam can be written as

$E_{out} = -j \exp(2\sigma\theta j) [1 \ -\sigma j]^T$. It shows that the helicity of the input CPL is reversed by the half waveplate and an extra phase difference is generated simultaneously which is equal to $\exp(2\sigma\theta j)$. This phase is the so-called PB phase which can be modulated by the optical axis θ of the waveplate. If the waveplate has a spatially variant optical axis distribution, the PB phase can be spatially modulated, which is similar to the modulation of optical path difference in conventional curved optical elements. LC, as one of the most widely used birefringence materials, is ideal for the PB phase modulation [13]. Furthermore, combining with the LC photoalignment technology [32], the optical axis distribution of the LC waveplate can be arbitrary controlled easily, which leads to the realisation of many LC PB phase optical elements including PB lens [33–35], polarisation grating and Q-plate [36].

The phase profile for circular lens is approximately a parabolic distribution [37], which can be described in a polar coordinate system (r, φ) as $\text{Phase}(r, \varphi) = \exp(j\pi r^2/\lambda f)$, in which f is the focal length of lens, λ is the wavelength of incident light. To build the LC PB lens, the corresponding optical axis orientation should be constructed as $\theta(r, \varphi) = \pi r^2/2\lambda f$. Since PB phase is circular polarisation sensitive, the phase modulation for different handedness of CPL can be written as $\text{Phase}(r, \varphi) = \exp(\pm j\pi r^2/\lambda f)$, which means the lens is simultaneously positive and negative for right-handed and left-handed CPL.

In a PB phase optical element, it has been shown that different phase distributions can be integrated in a single element [38]. Similar mechanism is used here to build the PB lens with spatially separated focuses. An extra linear phase distribution, for which the corresponding LC PB element is named polarisation grating, is integrated with the PB lens phase structure. The designed optical axis orientation of the new lens is described as $\theta = \pi x/p - \pi r^2/2\lambda f$. For incident CPL with $E_{in} = [1 \ \sigma j]^T$ and $\sigma = \pm 1$, the output light turns to be:

$$E_{out} = -j \exp \left[-j \left(\frac{2\sigma\pi x}{p} - \frac{\sigma\pi r^2}{\lambda f} \right) \right] \begin{bmatrix} 1 \\ -\sigma j \end{bmatrix}, \quad (2)$$

the first part $\exp(\mp j2\pi x/p)$ is a linear phase distribution along x direction, which can deflect light beams to different directions according to the $+$ and $-$ signs. The second phase part $\exp(\pm j\pi r^2/\lambda f)$ is the lens phase profile, in which the different signs represent that the lens is positive and negative for different handedness of CPL. The two phase parts are integrated in a single optical element, however, its optical function is similar

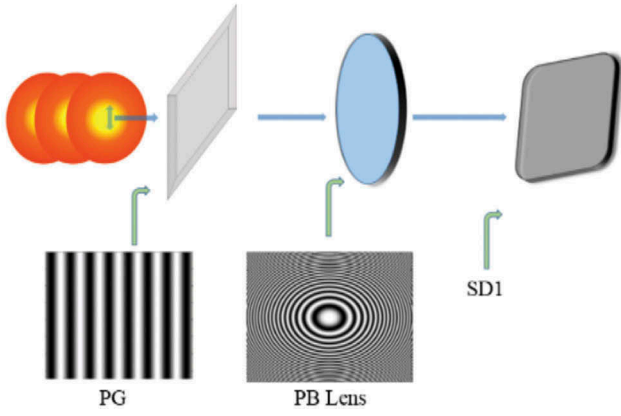


Figure 1. (Colour online) Fabrication steps of the new LC PB lens. The polarisation grating and PB lens are in fact stacked together to avoid the split of light caused by PG.

to two separated optical elements stacked together. When light passes through this newly designed optical element, it is expected that the two CPL beams will be separated and be focused in different spatial positions.

To produce the newly designed PB lens, the LC photoalignment technology is applied. We use the photoalignment material sulphonic azo-dye SD1 (from DIC Corp., Japan) with 0.5% solution dissolved in dimethylformamide in our experiment. This material has the property that when exposed to linearly polarised light, its aligned LC optical axis will be perpendicular to the polarisation of the exposed light whose wavelength is 450 nm and power density is 100 mW/cm² in our experiment. Therefore, the controlling of PB phase turns to be the controlling of polarisation of light exposed on the SD1 layer. An exposure set-up is designed as shown in Figure 1. In this figure, a conventional LC polarisation grating with $p_m = 4.1 \mu\text{m}$ and PB lens with $f_m = 420 \text{ mm}$ whose fabrication is based on polarisation holography set-up are stacked together. Linearly polarised laser light beam with wavelength 450 nm is illuminated passing through the two stacked elements, and then exposed on an SD1 layer which is spin-coated on a glass substrate at 800 rpm for 5 s and then 3-000 rpm for 30 s. Then the uniform thin SD1 film is put on a hotplate at 100°C for 30 min. The two stacked elements are playing the role of masks in this exposure set-up, and similar method is used in our previously experiment [39].

Jones matrix calculation is used to analyse the transformation process. The Jones matrix of the LC polarisation grating in half wave condition is:

$$M_{PG} = -j \begin{bmatrix} \cos \frac{2\pi x}{p_m} & \sin \frac{2\pi x}{p_m} \\ \sin \frac{2\pi x}{p_m} & -\cos \frac{2\pi x}{p_m} \end{bmatrix}, \quad (3)$$

in which the p_m represents the pitch of the polarisation grating. And the Jones matrix of the LC mask PB lens in half wave condition is:

$$M_{lens} = -j \begin{bmatrix} \cos \frac{\pi r^2}{\lambda f_m} & \sin \frac{\pi r^2}{\lambda f_m} \\ \sin \frac{\pi r^2}{\lambda f_m} & -\cos \frac{\pi r^2}{\lambda f_m} \end{bmatrix}, \quad (4)$$

wherein f_m is the focal length of the lens. The jones vector of the output beam turns out to be:

$$E_{out} = \begin{bmatrix} \cos(\frac{2\pi x}{p_m} - \frac{\pi r^2}{\lambda f_m} + \pi) \\ \sin(\frac{2\pi x}{p_m} - \frac{\pi r^2}{\lambda f_m} + \pi) \end{bmatrix}. \quad (5)$$

Considering the perpendicular relation between the exposed light's polarisation and the produced LC alignment direction, the resulted optical axis orientation distribution turns to be $\theta_m = 2\pi x/p_m - \pi r^2/\lambda f_m + \pi/2$. Compared with the targeted alignment orientation of the newly designed lens which is described as $\theta = \pi x/p - \pi r^2/2\lambda f$, the exposure set-up successfully produced the targeted structure with differences on the static $\pi/2$ shift and $p = p_m/2$, $f = f_m/2$, which are only some mathematical differences but by nature same for optical function.

Experimental process is described as below. First, the photoalignment material SD1 is spin-coated on a cleaned glass substrate. Then after baking for evaporating the solvent, the SD1 substrate is exposed with the exposure set-up shown in Figure 1. After that, the LC polymer RM257 (from Merck, Germany) added with 4 wt% of Irgacure 184 diluted in toluene at 1:9 in weight is repeatedly spin-coated on the SD1 film with 2500 rpm for 30 s and cured with UV light at a dosage of 2.5 J/cm² in nitrogen environment. When the coated film thickness designed for half wave retardation of the He-Ne laser 632.8 nm wavelength is satisfied, the newly designed PB lens is produced.

The schematic diagram of the theoretical and experimental LC PB lens observed under crossed polarisers is shown in Figure 2. As shown in Figure 2, (a) is the simulation diagram of the LC PB lens observed under the crossed polarisers; (b) is the micrograph of the fabricated LC PB lens observed by crossed polarisers; (c) is the enlarged figure of the simulation Figure 2(a); (d) is the enlarged figure of the experimental Figure 2(b).

A convex lens with focal length f_1 and a LC PB lens whose focal length is f_2 are successively illuminated by a right-handed circularly polarised beam $E_{in} = [1 \ -j]^T$ and the distance between the two lenses is D . The Jones matrix of the LC PB lens when its retardation is π equals to:

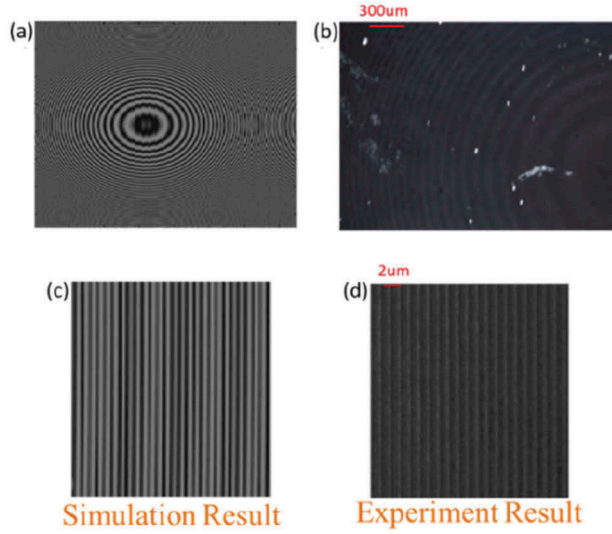


Figure 2. (Colour online) The schematic diagram of the theoretical and experimental LC PB lens observed under crossed polarisers. (a) and (b) are, respectively, simulation diagram and experimental micrograph of an LC PB lens with spatially separated focuses. (c) and (d) are the local magnified images of (a) and (b).

$$M = -j \begin{bmatrix} \cos 2\left(\frac{2\pi x}{p} - \frac{\pi r^2}{2\lambda f_2} + \frac{\pi}{2}\right) & \sin 2\left(\frac{2\pi x}{p} - \frac{\pi r^2}{2\lambda f_2} + \frac{\pi}{2}\right) \\ \sin 2\left(\frac{2\pi x}{p} - \frac{\pi r^2}{2\lambda f_2} + \frac{\pi}{2}\right) & -\cos 2\left(\frac{2\pi x}{p} - \frac{\pi r^2}{2\lambda f_2} + \frac{\pi}{2}\right) \end{bmatrix}. \quad (6)$$

Then we can obtain by a series of simple calculations that the focal length of the lens system is $f_3 = (f_1 - D)f_2/(f_1 + f_2 - D)$. A similarly derivation result is also valid that $f_4 = -(f_1 - D)f_2/(f_1 - f_2 - D)$ at the time the input light is left-handed circularly polarised.

The set-up of texture system is shown in Figure 3(a). A convex lens with focal length f_1 and a LC PB lens with focal length f_2 are successively illuminated by a linearly polarised beam, then the output beam split into two focused beams with two different focal length in 3D space.

In our testing set-up, the He-Ne laser source whose wavelength is 632.8nm is employed. Normal convex lens with $f_1 = 200$ mm and fabricated LC PB lens with $f_2 = 210$ mm are used. Distance between these two lenses is 80 mm. Hence, theoretically we can get by calculation that $f_3 \approx 76$ mm for right-handed circularly polarised beam and $f_4 \approx 280$ mm for left-handed circularly polarised beam. The texture result is shown in Figure 3. In our results, the measurement focal length for right-handed circularly polarised beam is 69 mm, while the measurement focal length for left-handed circularly polarised beam is 299 mm. By contrast, the experimental results are very close to the theoretical results.

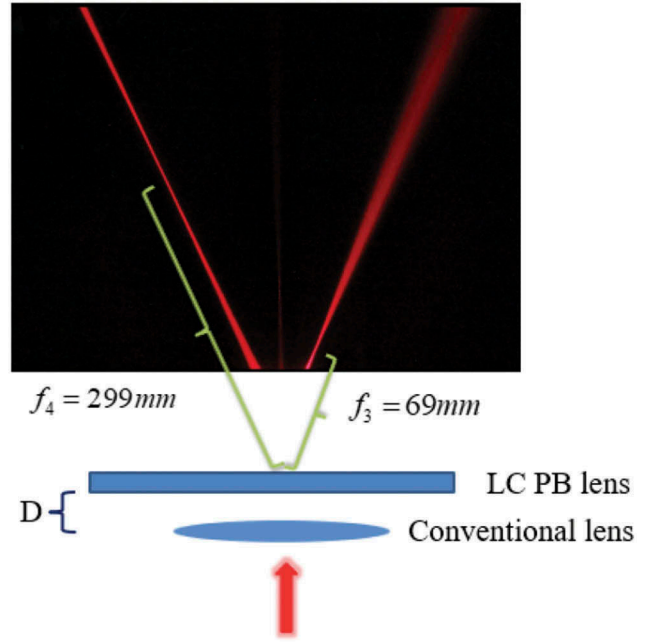


Figure 3. (Colour online) Testing set-up and results of the LC PB lens.

The imaging test of our lens system is as shown in Figure 4. The light path diagram of the testing progress is shown in Figure 4(a). The position of the observer for Figure 4(b, c) is marked out in Figure 4(a). A pentagram is used as the texting pattern in Figure 4(b) and an abbreviation of hologram ‘HG’ is used in Figure 4(c). They were put in front of the lenses and illuminated by a linearly polarised He-Ne laser with wavelength = 632.8 nm. We can see from the images shown in Figure 4 that the brightness of the images varies with the changes of the observer’s locations, and the imaging sizes are different for the same object in two separated light paths. These results show that the focal lengths of the separated light paths are different.

In summary, a LC PB lens with spatially separated focuses is proposed and fabricated. That lens is an inhomogeneous wave plate whose optical axis orientation is an integration of PB lens and polarisation grating. Once illuminated by linearly polarised beam, it can generate two beams propagated towards two opposite directions about the central axis. The generated spatially separated beams possess opposite focal lengths. When combined with normal convex lens and illuminated by a linearly polarised beam, the two emergent light beams become all convergent and the two focuses are separated in three-dimension space. Moreover, the focal lengths of the lens system can be artificially controlled by adjusting the distance between our new lens and the conventional lens. Equipped with such special optical features, the proposed LC PB lens will

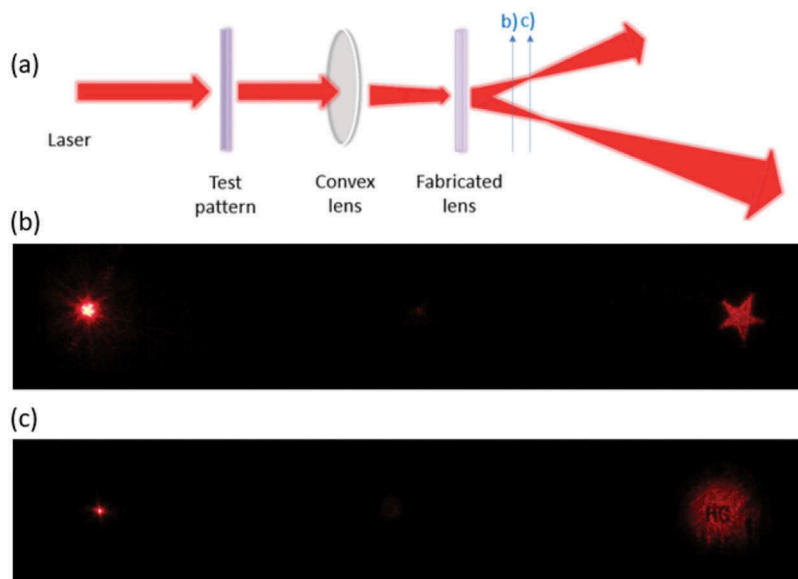


Figure 4. (Colour online) Texture of the LC PB lens. (a) The light path diagram of the testing progress and the position of the observer in Figure 4(b, c). (b) Images observed while a pentagram is set as the testing pattern; (c) While the testing pattern is the abbreviation of hologram 'HG'.

be widely used in optical manipulation and space imaging areas.

The LC PB lens, which is equipped with above special optical features, brilliant optical quality and convenient fabrication steps, possesses a great potential to find widely applications in imaging field.

Disclosure statement

No potential conflict of interest was reported by the authors.

Funding

This work is supported by the National Natural Science Foundation of China [61605046, 11574079], Natural Science Foundation of Hunan Province [2018JJ3069] and the Fundamental Research Funds for the Central Universities. This work is also supported by the State Key Laboratory of applied optics.

References

- [1] Heng H, Vepachedu V. Recent development of transient electronics. *TAML*. 2016;6(1):21–31.
- [2] Miyamoto K. Fish eye lens. *J Opt Soc Am*. 1964;54(8):1060–1061.
- [3] Kumar V, Shrivastava RL, Untawale SP. Fresnel lens: a promising alternative of reflectors in concentrated solar power. *Renew Sust Energ Rev*. 2015;44:376–390.
- [4] Koomen M, Scolnik R, Tousey R. A study of night Myopia. *J Opt Soc Am*. 1951;41(2):80–90.
- [5] Riza NA, DeJule MC. Three-terminal adaptive nematic liquid-crystal lens device. *Opt Lett*. 1994;19(14):1013–1015.
- [6] Naumov AF, Loktev MY, Guralnik IR, et al. Liquid-crystal adaptive lenses with modal control. *Opt Lett*. 1998;23(13):992–994.
- [7] Kong X, Khan AA, Kidambi PR, et al. Graphene based ultra-thin flat lenses. *ACS Photonics*. 2015;2(2):200–207.
- [8] Ke Y, Liu Y, Zhou J, et al. Optical integration of Pancharatnam-Berry phase lens and dynamical phase lens. *Appl Phys Lett*. 2016;108(10):101–102.
- [9] Azad AK, Efimov AV, Ghosh S, et al. Ultra-thin meta-surface microwave flat lens for broadband applications. *Appl Phys Lett*. 2017;110(22):611–617.
- [10] Chen HT, Taylor AJ, Yu N. A review of metasurfaces: physics and applications. *Rep Prog Phys*. 2016;79(7):076401.
- [11] Genevet P, Capasso F. Holographic optical metasurfaces: a review of current progress. *Rep Prog Phys*. 2015;78(2):024401.
- [12] Marrucci L, Manzo C, Paparo D. Pancharatnam-Berry phase optical elements for wave front shaping in the visible domain: switchable helical mode generation. *Appl Phys Lett*. 2006;88(22):1141.
- [13] Hasman E, Kleiner V, Biener G, et al. Polarization dependent focusing lens by use of quantized Pancharatnam-berry phase diffractive optics. *Appl Phys Lett*. 2003;82(3):328–330.
- [14] Lee Y, Tan G, Zhan T, et al. Recent progress in Pancharatnam-berry phase optical elements and the applications for virtual/augmented realities. *Opt Data Process Storage*. 2017;3:79–88.

- [15] Vieu C, Carcenac F, Pépin A, et al. Electron beam lithography: resolution limits and applications. *Appl Surf Sci.* **2000**;164:111–117.
- [16] Yu N, Capasso F. Flat optics with designer metasurfaces. *Nat Mater.* **2014**;13(2):139–150.
- [17] Yaroshchuk O, Reznikov Y. Photoalignment of liquid crystals: basics and current trends. *J Mater Chem.* **2011**;22(2):286–300.
- [18] Schadt M, Schmitt K, Kozinkov V, et al. Surface-induced parallel alignment of liquid crystals by linearly polymerized photopolymers. *Jpn J Appl Phys.* **2014**;51(7):2155–2164.
- [19] Ichimura K. Photoalignment of liquid-crystal systems. *Chem Rev.* **2000**;100(5):1847–1874.
- [20] Lee YH, Peng F, Wu ST. Fast-response switchable lens for 3D and wearable displays. *Opt Express.* **2016**;24(2):1668–1675.
- [21] Jacques SL, Ramellaroman JC. Imaging superficial tissue layers using polarized light with a hand-held camera. *Proc Spie.* **2003**;5254:14–23.
- [22] Soloviev VY, Zacharakis G, Spiliopoulos G, et al. Tomographic imaging with polarized light. *J Opt Soc Am A.* **2012**;29(6):980–988.
- [23] Bimber O, Emmerling A. Multifocal projection: a multiprojector technique for increasing focal depth. *IEEE T Vis Comput Gr.* **2006**;12:658–667.
- [24] Pan S, Yao J. Multichannel optical signal processing in NRZ systems based on a frequency-doubling optoelectronic oscillator. *IEEE J Sel Top Quant.* **2010**;16(5):1460–1468.
- [25] Gutiérrez-Vega JC. Pancharatnam-Berry phase of optical systems. *Opt Lett.* **2011**;36(7):1143–1145.
- [26] Vanholsbeeck F, Lippok N, Nielsen P, et al. Instantaneous quadrature components or Jones vector retrieval using the Pancharatnam-Berry phase in frequency domain low-coherence interferometry. *Opt Lett.* **2012**;37(15):3102–3104.
- [27] Yirmiyahu Y, Niv A, Biener G, et al. Vectorial vortex mode transformation for a hollow waveguide using Pancharatnam-Berry phase optical elements. *Opt Lett.* **2006**;31(22):3252–3254.
- [28] Bomzon Z, Biener G, Kleiner V, et al. Space-variant Pancharatnam-Berry phase optical elements with computer-generated subwavelength gratings. *Opt Lett.* **2002**;27(13):1141–1143.
- [29] Wang X, Yang W, Liu Z, et al. Switchable Fresnel lens based on hybrid photo-aligned dual frequency nematic liquid crystal. *Opt Mater Express.* **2017**;7(1):8–15.
- [30] Niv A, Biener G, Kleiner V, et al. Propagation-invariant vectorial Bessel beams obtained by use of quantized Pancharatnam-Berry phase optical elements. *Opt Lett.* **2004**;29(3):238–240.
- [31] Huang B, Wang Q, Jiang G, et al. Wavelength-locked vectorial fiber laser manipulated by Pancharatnam-Berry phase. *Opt Express.* **2017**;25(1):30–38.
- [32] Chigrinov VG. Photoalignment and photopatterning in liquid crystal photonics. *Proc SPIE.* **2012**;8279(1):20.
- [33] Roux FS. Geometric phase lens. *J Opt Soc Am A.* **2006**;23(2):476–482.
- [34] Gao K, Hh C, Bhowmik AK, et al. Thin-film Pancharatnam lens with low f-number and high quality. *Opt Express.* **2015**;23(30):26086.
- [35] Zhan T, Yh L, Wu ST. High-resolution additive light field near-eye display by switchable Pancharatnam-Berry phase lenses. *Opt Express.* **2018**;26(4):4863.
- [36] Marrucci L. Rotating light with light: generation of helical modes of light by spin-to-orbital angular momentum conversion in inhomogeneous liquid crystals. *Proc SPIE.* **2007**;488(1):148–162.
- [37] Campbell MC. Measurement of refractive index in an intact crystalline lens. *Vision Res.* **1984**;24(5):409–415.
- [38] Alwin M, Tam W, Fan F, et al. Bifocal optical-vortex lens with sorting of the generated nonseparable spin-orbital angular-momentum states. *Phys Rev Appl.* **2017**;7(3):0304010–0304010.
- [39] Asatryan K, Galstian T, Chigrinov V, et al. Optical polarization grating induced liquid crystal micro-structure using azo-dye command layer. *Opt Express.* **2006**;14(22):10558–10564.